

OPEN ACCESS

EDITED BY
Sung-Kwon Moon,
Chung-Ang University, Republic of Korea

REVIEWED BY Chunmei Sai, Jining Medical University, China Ahmad Bikharudin, Okayama University, Japan

*CORRESPONDENCE
Ying Wang,

☑ yingwang912@163.com

RECEIVED 15 August 2025 ACCEPTED 29 September 2025 PUBLISHED 17 October 2025

CITATION

Lin B, Zhang M and Wang Y (2025) Alkaloid-driven multi-target synergy of *Tripterygium wilfordii* polyglycosides overcomes cisplatin resistance in ovarian cancer by coordinated inhibition of PTPN11/EGFR/JAK signaling. *Front. Pharmacol.* 16:1686526. doi: 10.3389/fphar.2025.1686526

COPYRIGHT

© 2025 Lin, Zhang and Wang. This is an openaccess article distributed under the terms of the Creative Commons Attribution License (CC BY). The use, distribution or reproduction in other forums is permitted, provided the original author(s) and the copyright owner(s) are credited and that the original publication in this journal is cited, in accordance with accepted academic practice. No use, distribution or reproduction is permitted which does not comply with these terms.

Alkaloid-driven multi-target synergy of *Tripterygium wilfordii* polyglycosides overcomes cisplatin resistance in ovarian cancer by coordinated inhibition of PTPN11/EGFR/JAK signaling

Bing Lin^{1,2}, Minxin Zhang¹ and Ying Wang^{1,2}*

Objective: *Tripterygium wilfordii* polyglycoside (TWP) is a standardized extract from *T. wilfordii* Hook. f. and an oral prescription drug approved by the China Food and Drug Administration (now NMPA) for clinical use in inflammatory and autoimmune diseases. Leveraging its existing clinical approval, elucidating its anti-tumor mechanisms has high translational value for expanding its indications into oncology. This study aimed to clarify whether TWP can overcome cisplatin resistance in ovarian cancer and to explore a mechanism potentially centered on its alkaloid constituents through an integrated "prediction-validation" strategy. **Methods:** UPLC-QTOF-MS was used for chemical profiling. Network pharmacology predicted putative targets, validated by GEO transcriptomic datasets. Key alkaloid-target interactions were examined by molecular docking and 100-ns MD simulations. *In vitro* assays (CCK-8, Annexin V-FITC/PI, Western blot) in cisplatin-resistant A2780/DDP cells confirmed phenotypic and mechanistic effects.

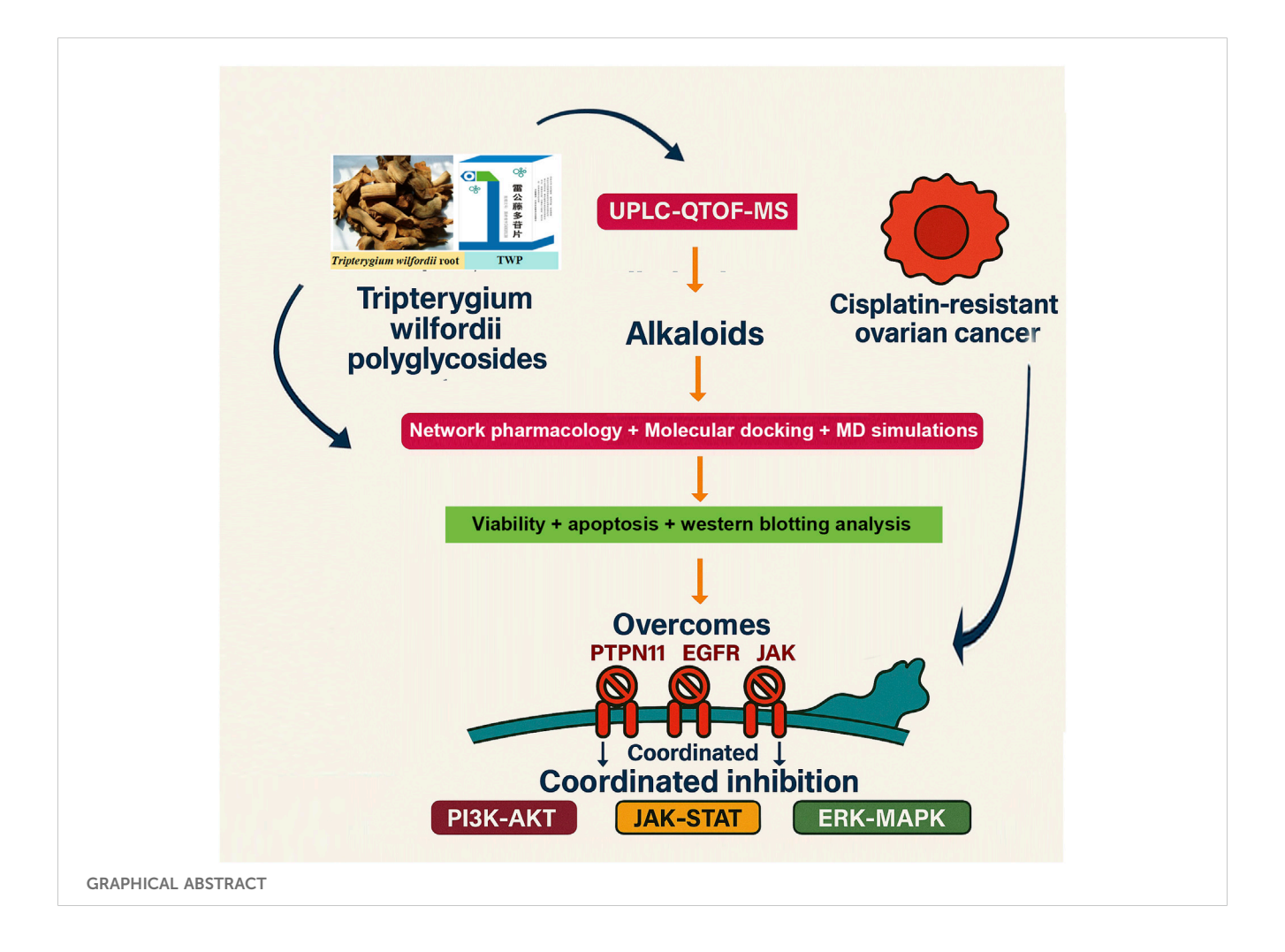
Results: Thirty-eight constituents were identified, including 18 alkaloids. Five core targets (EGFR, JAK1, JAK2, PTPN11, SRD5A1) were pinpointed by network—clinical integration. Several alkaloids ranked among the top compounds by network degree, exhibited strong predicted binding affinities ($\Delta G \leq -7$ kcal/mol), and formed stable complexes in molecular dynamics simulations. Functionally, TWP reduced viability, induced apoptosis, and de-phosphorylated EGFR, JAK1/2, and PTPN11, downregulated SRD5A1, and suppressed PI3K-AKT, JAK-STAT, and ERK-MAPK signaling.

Conclusion: Our findings suggest that alkaloids in TWP may exert multi-target synergy to disrupt key survival pathways driving cisplatin resistance in ovarian cancer. These mechanistic insights not only rationalize its observed anti-tumor activity but also support its potential clinical repurposing from an approved anti-inflammatory drug to an oncology therapeutic.

KEYWORDS

Tripterygium wilfordii polyglycoside, ovarian cancer, cisplatin resistance, network pharmacology, multi-target therapy, alkaloids

¹Department of Pharmacy, Fuzong Clinical Medical College of Fujian Medical University, Fuzhou, China, ²Department of Pharmacy, 900th Hospital of PLA Joint Logistic Support Force, Fuzhou, China



1 Introduction

Ovarian cancer remains a formidable challenge in gynecological oncology, characterized by insidious progression, late-stage diagnosis, and high mortality rates. Despite initial responsiveness to cytoreductive surgery and platinum-based chemotherapy, approximately 70% of patients with advanced disease experience recurrence within 18 months, subsequently developing chemoresistance that severely compromises therapeutic efficacy and survival outcomes (Murphy et al., 2021). This escalating crisis of platinum resistance underscores an urgent unmet need for novel therapeutic strategies capable of overcoming treatment-refractory disease.

In this context, Traditional Chinese Medicine (TCM) has garnered significant attention for its holistic, multi-component, and multi-target therapeutic philosophy. Accumulating evidence has validated the efficacy of various TCM-derived agents against ovarian cancer. For instance, compounds such as berberine and curcumin have been shown to suppress tumor progression and induce apoptosis by modulating critical oncogenic pathways like PI3K/Akt and EGFR, with notable efficacy even in cisplatin-resistant cells (Zhang et al., 2025; Liu et al., 2023). Furthermore, other agents like ginsenoside Rg6 specifically target chemoresistance, enhancing cisplatin sensitivity through mechanisms such as the induction of

autophagy (Xue et al., 2025). These examples highlight the capacity of TCM-derived compounds to combat ovarian cancer through diverse and synergistic mechanisms.

Among TCM-derived agents, Tripterygium polyglycoside (TWP) is a standardized oral extract from T. wilfordii Hook. f. and an approved prescription drug by the China Food and Drug Administration (now NMPA) for clinical use in inflammatory and autoimmune diseases. Previous studies have demonstrated that TWP possesses significant anti-tumor effects, including the ability to inhibit ovarian cancer cell proliferation, suppress migration and invasion, and reverse cisplatin resistance in drug-resistant cell lines (Zhan et al., 2023; Ma et al., 2023). Nevertheless, the precise molecular mechanisms underlying these multi-faceted effects remain incompletely elucidated. Notably, while the anti-tumor activity of TWP is often attributed to its well-documented diterpenoid constituents, the specific contribution of its large family of alkaloid compounds—a class known for potent bioactivity as exemplified by agents like berberine—remains a critical and under explored area, impeding the rational optimization of TWP-based regimens.

To bridge this critical knowledge gap, we employed a multidimensional integrative approach combining UPLC/Q-TOF-MS phytochemical profiling, network pharmacology, microarraybased transcriptomic analysis, and advanced molecular modeling

techniques. This strategy enabled systematic deconvolution of TWP's chemical composition, identification of its bioactive constituents, prediction of therapeutic targets, and validation of their clinical relevance in ovarian cancer pathogenesis. Based on our initial objective to investigate the under explored components of TWP, our findings compellingly demonstrate that alkaloids, far from being secondary players, constitute a primary class of active components driving TWP's anti-ovarian cancer effects. This was evidenced by their superior efficacy in targeting key chemoresistance pathways in our network pharmacology models. Through integrated network analysis and clinical transcriptomic data, we identified five core targets (EGFR, JAK1, JAK2, PTPN11, and SRD5A1) that are differentially expressed in ovarian cancer tissues and serve as central nodes in TWP's mechanism of action. Subsequent molecular docking and dynamics simulations confirmed stable, high-affinity binding between TWP alkaloids and these targets, providing structural insights into their interactions. Crucially, experimental validation demonstrated that TWP simultaneously modulates these targets to coordinately suppress PI3K-AKT, JAK-STAT, and ERK-MAPK signaling pathways, thereby inducing apoptosis and overcoming cisplatin resistance in ovarian cancer cells.

This study elucidates a novel mechanistic framework by which TWP's alkaloid constituents exhibit multi-target synergistic effects against platinum-resistant ovarian cancer. By deliberately shifting the scientific focus from the well-trodden path of diterpenoids, our findings establish that TWP's alkaloids play a pivotal, not merely a supplementary, role in modulating key molecular targets (EGFR, JAK1/2, PTPN11, SRD5A1) and associated signaling pathways (PI3K-AKT, JAK-STAT, and ERK-MAPK). These results complement existing knowledge of TWP's anti-tumor properties and provide new insights for developing more effective therapeutic strategies against chemoresistant ovarian cancer.

2 Materials and methods

2.1 Chemicals and reagents

Chromatographic-grade methanol and acetonitrile were obtained from Merck and Sigma-Aldrich (Darmstadt, Germany). Deionized water was prepared using a Milli-Q system (Millipore, Bedford, MA, United States). Tripterygium wilfordii polyglycoside (TWP) was provided by Jiangsu Meitong Pharmaceutical Co., Ltd. (Jiangsu, China). RIPA lysis buffer was from Beyotime (Shanghai, China). Primary antibodies: SRD5A1 (ab167606, 1:2000, rabbit; Abcam, Waltham, MA, United States); JAK1 (PT0658R, 1:1000, rabbit), JAK2 (PT0503R, 1:2000, rabbit), Bax (PT0301R, 1:2000, rabbit), Bcl-2 (PT0487R, 1:2000, rabbit), phospho-STAT3 (Tyr705; YP0251, 1:2000, rabbit), STAT3 (PT0911R, 1:2000, rabbit), and Akt (PT0654R, 1:2000, mouse) from ImmunoWay (Jiangsu, China); cleaved caspase-3 (#96641, 1:1000, rabbit), EGFR (#4267, 1:1000, rabbit), phospho-EGFR (#3777, 1:1000, rabbit), PTPN11/SHP2 (#3397, 1:2000, rabbit), phospho-PTPN11 (#5431, 1:1000, rabbit), phospho-ERK1/2 (#4370, 1:2000, rabbit), ERK1/2 (#4695, 1:2000, rabbit) from Cell Signaling Technology (Danvers, MA, United States); phospho-Akt (AA329, 1: 2000, rabbit), phospho-JAK1 (AF5857, 1:2000, rabbit), phospho-JAK2 (AF1486, 1:2000, rabbit), and GAPDH (AF0006, 1:10000, mouse) from Beyotime (Shanghai, China).

2.2 UPLC/Q-TOF-MS profiling

2.2.1 Sample preparation

TWP (20.0 mg) was weighed into a 10 mL volumetric flask, dissolved by sonication in methanol, brought to volume, vortex-mixed, and filtered (0.22 μ m).

2.2.2 LC-MS conditions

Chromatography used an Agilent 1290 UPLC with a Waters ACQUITY UPLC XBridge BEH C18 column (2.1 × 50 mm, 1.7 μ m). Mobile phase: acetonitrile (A) and water with 0.1% formic acid (B), 0.3 mL/min, 35 °C. Gradient: 0–10 min, 20% A; 10–60 min, 20% 45% A; 60–90 min, 45% A; 90–120 min, 45%–85% A; 120–150 min, 85% A; 150–170 min, 85%–90% A. Injection: 5 μ L.

An Agilent 6520 Q-TOF with ESI in positive mode acquired mass spectra (source 350 °C; drying gas 10 L/min; nebulizer 40 psi; fragmentor 130 V; capillary 3500 V; 1 spectrum/s, 2 GHz dynamic range; m/z 50–1200). MS/MS used the same source settings.

2.2.3 Compound identification

A Tripterygium database was compiled from CNKI, Wanfang, PubMed, Web of Science, SciFinder, and Reaxys. Constituents were annotated by accurate mass, MS/MS fragmentation, and retention time, and confirmed against reference standards when available. Molecular formulae were inferred from exact mass and isotopic patterns. Compounds were classified as alkaloids, diterpenoids, triterpenoids, or other.

2.3 Target prediction and disease target collection

Active constituents were selected from the 38 identified compounds based on the criteria of Oral Bioavailability (OB) \geq 30% and Drug-Likeness (DL) \geq 0.18, yielding 26 compounds for target prediction. Human targets were predicted using SwissTargetPrediction (probability \geq 0.7), excluding low-confidence predictions. Ovarian cancer-associated genes were retrieved from GeneCards, OMIM, and CTD using the keywords "ovarian neoplasm," "ovarian tumor," and "ovarian carcinoma." Duplicates and non-human entries were removed. Overlap with TWP-predicted targets was computed in R (v4.2.0, VennDiagram); UniProt IDs were used downstream.

2.4 Network construction and analysis

A compound–target bipartite network was built in Cytoscape 3.9.0. Topological parameters (degree, betweenness, closeness) prioritized key constituents and targets. Overlapping targets were submitted to STRING v11.5 (*Homo sapiens*; minimum interaction score ≥0.4) including experimental, curated database, and textmining evidence (neighbourhood, gene fusion, and co-occurrence excluded). Networks were visualized in Cytoscape. CytoHubba identified hub genes using Maximal Clique Centrality (MCC), and MCODE detected densely connected subnetworks using standard parameters (degree cutoff = 2, node score cutoff = 0.2, k-core = 2, max depth = 100).

2.5 Functional enrichment

GO and KEGG enrichment used DAVID 6.8 (H. sapiens background), with p < 0.01 and Benjamini–Hochberg correction. GO terms were categorized into biological process (BP), cellular component (CC), and molecular function (MF). The top 10 terms in each category were visualized as bubble plots (ggplot2, enrichplot), with bubble size denoting gene count and color indicating $-\log 10$ (adjusted p).

2.6 Molecular docking and MD simulations

The ten highest-ranked constituents by network centrality were docked to five core targets (EGFR, JAK1, JAK2, PTPN11, SRD5A1). Ligand 3D structures were retrieved from PubChem (SDF), protonated at pH 7.4, and minimized with MMFF94 (Open Babel 3.1). Protein structures: EGFR (PDB: 1M17); JAK1 (PDB: 4E5W) and JAK2 (PDB:3IO7) kinase domains (validated highresolution human structures with co-crystallized inhibitors); PTPN11 (PDB: 3MOW); SRD5A1 (PDB: 7C83) modeled using the AlphaFold structure (UniProt Q13675; AF-Q13675-F1) due to the lack of a suitable experimental structure. Proteins were prepared in AutoDockTools 1.5.6 (removal of waters/non-native ligands, addition of polar hydrogens, Gasteiger charges). Grid boxes were centered on catalytic pockets. Docking used AutoDock Vina 1.2.2 (exhaustiveness = 8; 20 runs/ligand). Lowest-energy poses (ΔGbind) were retained; binding modes were visualized in PyMOL 3.0 and annotated with LigPlot+ 2.2.

For MD, 100-ns all-atom simulations were performed in GROMACS 2024.3. Proteins used Amber99SB-ILDN; ligands were parameterized with GAFF via ACPYPE/Antechamber (AM1-BCC charges). Complexes were solvated in a dodecahedral box of SPC216 water with 0.15 M NaCl. Energy minimization employed steepest descent (5,000 steps) to max force <1000 kJ/mol/nm. Equilibration: 500 ps NVT at 300 K (heavy-atom restraints) and 1,000 ps NPT at 300 K with gradually reduced restraints. Production: 300 K, 1 bar, v-rescale thermostat (τ T = 0.1 ps), Parrinello–Rahman barostat (τ P = 2.0 ps). PME handled electrostatics (real-space cutoff 1.0 nm); van der Waals used a forceswitch at 0.9–1.0 nm. Bonds to hydrogens were constrained with LINCS (2 fs time step). Trajectories were saved every 10 ps? RMSD and RMSF were computed with GROMACS tools and plotted in R.

2.7 Microarray analysis and experimental validation

2.7.1 Clinical transcriptomics

Four GEO datasets (GSE18520, GSE26712, GSE27651, GSE54388) were analyzed. Preprocessing and differential expression used limma (background correction, normalization, probe summarization). DEGs were defined as adjusted p < 0.05 and |log2| fold change|log2| 1. DEGs were cross-referenced with hub genes to derive core targets.

2.7.2 Cell culture and treatments

Human ovarian cancer SKOV3 and cisplatin-resistant A2780/DDP cells (Changsha Abiowell Biotechnology Co., Ltd., Changsha,

China) were cultured in DMEM with 10% FBS and 1% penicillin/ streptomycin at 37 °C in 5% CO₂. TWP stocks were prepared in DMSO; final DMSO \leq 0.1%. Cisplatin was used at 10 μ M where indicated.

2.7.3 Cell viability

CCK-8 (Beyotime, Shanghai, China) assessed viability. Cells were seeded in 96-well plates (5 \times 10³ cells/well), incubated overnight, and treated with cisplatin (10 μ M) and TWP (0, 5, 10, 20 μ g/mL) for 24 h. CCK-8 reagent (10 μ L) was added for 2 h at 37 °C; absorbance at 450 nm was read (BioTek Instruments).

2.7.4 Apoptosis

Annexin V-FITC/PI staining (Elabscience) followed the manufacturer's protocol. After 24 h TWP (0, 5, 10, 20 μ g/mL), cells were harvested, washed, stained for 15 min at room temperature in the dark, and analyzed on a CytoFLEX nano flow cytometer (Beckman Coulter).

2.7.5 Western blot

Total protein was extracted with RIPA plus protease/ phosphatase inhibitors (Wuhan Cobio, Wuhan, China) and quantified by BCA (Wuhan Cobio). Equal protein (30 μg) was separated by 10% SDS-PAGE, transferred to PVDF (Millipore), blocked with 5% non-fat milk (1 h, room temperature), and incubated overnight at 4 °C with primary antibodies against EGFR, phospho-EGFR, JAK1, phospho-JAK1, JAK2, phospho-JAK2, PTPN11, phospho-PTPN11, SRD5A1, Akt, phospho-Akt, STAT3, phospho-STAT3, ERK1/2, phospho-ERK1/2, Bcl-2, Bax, cleaved caspase-3, and GAPDH. HRP-conjugated secondary antibodies (1:5000) and ECL (GE Healthcare) were used for detection. Bands were quantified with ImageJ v1.53t and normalized to GAPDH.

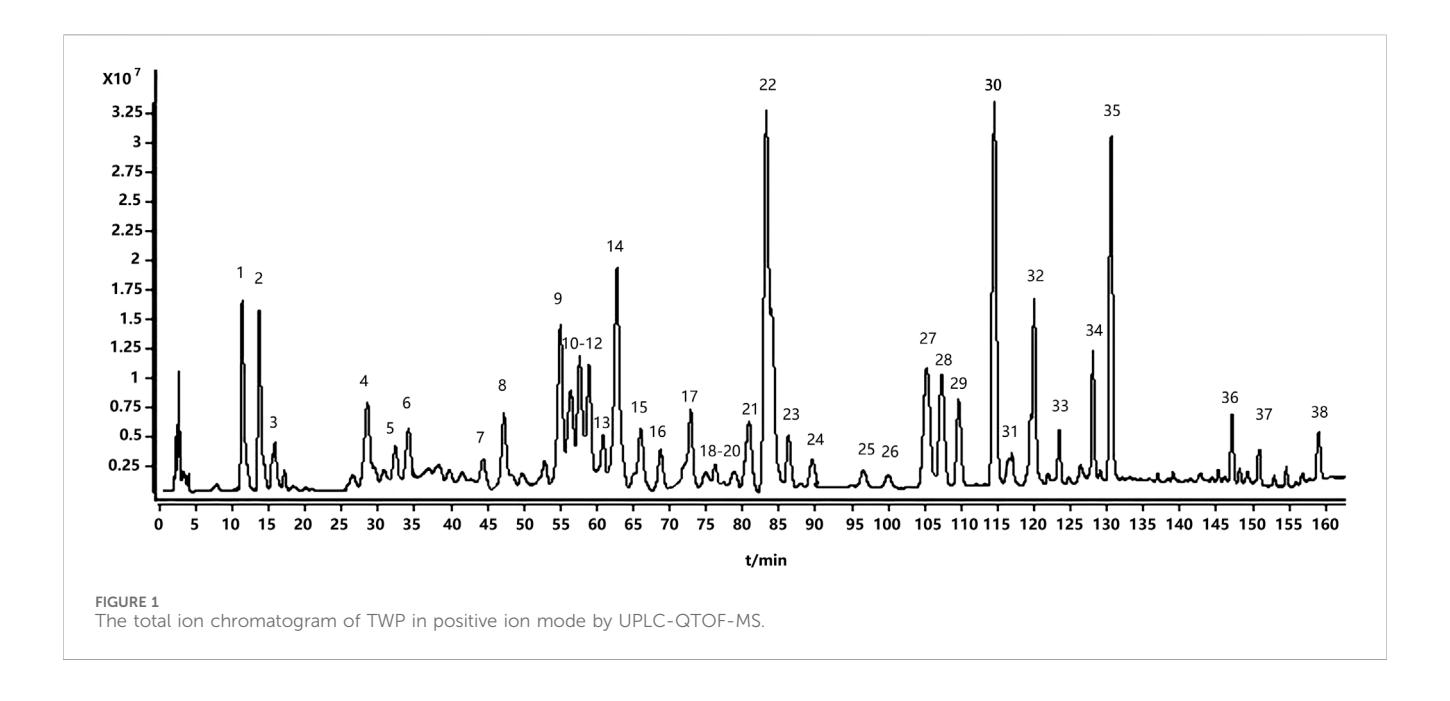
2.8 Statistical analysis

Unless otherwise indicated, data represent mean \pm SD from n = 3 independent experiments (each with \geq 3 technical replicates). Oneway ANOVA with Tukey's *post hoc* test was used for multiple comparisons (GraphPad Prism 8.0). Two-sided p < 0.05 was considered statistically significant.

3 Results

3.1 UPLC/Q-TOF-MS-based qualitative profiling of TWP

UPLC/Q-TOF-MS in positive and negative ion modes identified 38 constituents; positive mode yielded superior signal and was used for detailed analysis (Figure 1). Based on $[M + H]^+$ ions, fragmentation patterns, standards, and literature, we annotated 18 alkaloids, 8 diterpenoids, 8 triterpenoids, and 4 others (Table 1). The fact that alkaloids represent the most numerous chemical class identified (18 of 38 total compounds) prompted us to hypothesize their significant contribution to TWP's overall bioactivity. This hypothesis was subsequently tested and strongly



supported by our network pharmacology analysis (see Section 3.3), which revealed that alkaloid constituents were the most highly connected nodes in the compound-target network, suggesting they are the primary mediators of TWP's effects on ovarian cancer targets.

3.2 Screening for ovarian cancer-related targets of TWP

Potential molecular targets of TWP constituents were predicted using SwissTargetPrediction, yielding 743 unique targets. Ovarian cancer-associated genes (n = 5,156) were curated from GeneCards, OMIM, and CTD databases. Venn diagram analysis identified 242 overlapping targets between TWP-predicted targets and ovarian cancer-related genes (Figure 2A), suggesting these may mediate TWP's therapeutic effects against ovarian cancer.

3.3 Network analysis of TWP and ovarian cancer targets

A compound-target network was constructed to visualize interactions between TWP constituents and their predicted targets. The bipartite network (Figure 2B) comprised 268 nodes (26 compounds, 242 targets) and 1,274 edges, reflecting TWP's multi-component, multi-target pharmacology. Topological analysis identified highly connected compounds, likely representing key pharmacologically active constituents. The top 10 compounds by degree (Table 2) were predominantly alkaloids (e.g., wilfordinine A, wilfordine, wilfornine A, wilfortrine, euojaponine D), consistent with chemical profiling and suggesting alkaloids as primary mediators of TWP's anti-ovarian cancer effects.

3.4 PPI network analysis

A PPI network of the 242 overlapping targets was constructed using the STRING database (Figure 3A). To identify critical functional modules, the network was analyzed using both CytoHubba and MCODE plugins. MCODE identified three densely connected subnetworks: Subnetwork 1 (Score: 10.364): Enriched in signaling pathways (12 nodes, 57 edges), featuring JAK1, JAK2, EGFR, PIK3CA, PIK3CB, and PTPN11. Subnetwork 2 (Score: 9.000): Associated with steroid hormone biosynthesis (9 nodes, 36 edges), including SRD5A1, CYP17A1, and AKR1C3. Subnetwork 3 (Score: 5.500): Involved in inflammation/apoptosis regulation (13 nodes, 27 edges), containing PRKCA, PRKCB, HSP90AA1, and SRC. Concurrently, CytoHubba identified the top 10 hub genes by degree centrality (Figure 3B): SRD5A1, PTPN11, PIK3CA, PIK3CB, JAK2, EGFR, PTPN6, JAK1, AKR1C3, and CYP17A1. These hub genes were integral to the MCODE subnetworks (e.g., SRD5A1 and CYP17A1 in Subnetwork 2; JAK2 and EGFR in Subnetwork 1). Table 3 details their functions, targeting compounds, and pathways. Notably, these genes converge on cancer-related pathways (JAK-STAT, PI3K-Akt, tyrosine kinase signaling), underscoring their role in TWP's anti-ovarian cancer effects.

3.5 GO enrichment and KEGG pathway analysis

GO and KEGG analyses of the 242 targets identified 693 biological processes (BP), 95 cellular components (CC), 187 molecular functions (MF), and 167 KEGG pathways significantly enriched (p < 0.01). Top enriched terms (Figure 4) included: BP: Protein phosphorylation, response to xenobiotic stimuli, peptidyl-serine phosphorylation, inflammatory response (Figure 4A). MF: Protein kinase activity, ATP binding, enzyme

TABLE 1 UPLC-QTOF-MS identification of 38 chemical constituents in TWP.

Peak no.	Compound name	Molecular formula	[M + H] ⁺ /[M + Na] ⁺ (m/z)	RT/ min	DL
1	Triptofordinine A2	$C_{41}H_{43}NO_{12}$	742.7796	11.25	0.47
2	Wilforjine	C ₃₆ H ₄₅ NO ₁₇	764.2841	14.08	0.72
3	Hypodiol	$C_{30}H_{50}O_{2}$	443.1555	15.78	0.18
4	Wilfordinine B	C ₃₈ H ₄₇ NO ₁₉	822.2888	28.85	0.74
5	Neoeuonymine	C ₃₆ H ₄₅ NO ₁₇	764.2824	32.55	0.54
6	Tripterifordin	$C_{20}H_{30}O_3$	319.2307	34.44	0.49
7	Wilfordinine A	C ₃₆ H ₄₅ NO ₁₇	764.2828	44.42	0.88
8	Euonine	C ₃₈ H ₄₇ NO ₁₈	806.2956	47.12	0.2
9	Triptonodiol	$C_{21}H_{30}O_4$	347.2259	49.95	0.42
10	Wilfortrine	C ₄₁ H ₄₇ NO ₂₀	874.2866	51.15	0.15
11	Tripterygiol	$C_{22}H_{28}O_{8}$	421.4529/443.1688	57.52	0.16
12	Hypoglaunine A	$C_{41}H_{47}NO_{20}$	874.2832	59.05	0.78
13	Euonine	C ₃₈ H ₄₇ NO ₁₈	806.295	60.75	0.2
14	Triptoquinone B	$C_{20}H_{26}O_4$	331.1936	62.85	0.32
15	2α, 3α, 23-trihydroxyursane-12-en-28 oic acid	$C_{30}H_{48}O_5$	489.3245	65.93	0.71
16	Wilfordine	Wilfordine $C_{43}H_{49}NO_{19}$		884.304 68.91	
17	9'-O-Acetylwilfortrine	$C_{43}H_{49}NO_{21}$	916.2919	73.02	0.56
18	Hypoglaunine D	$C_{41}H_{47}NO_{19}$	858.2891	75.05	0.94
19	Aurantiamide acetate	$C_{27}H_{28}N_2O_4\\$	445.1561	76.14	0.52
20	Euojaponine D	$C_{41}H_{47}NO_{17}$	826.2944	79.26	0.7
21	Wilfornine A	$C_{45}H_{51}NO_{20}$	926.3116	80.78	0.4
22	Wilfordinine F	$C_{43}H_{49}NO_{18}$	868.308	83.81	1.1
23	2β,22β-Dihydroxy-3,21-dioxo-24-carboxyl-29-nor-friedelan methyl ester	$C_{30}H_{46}O_{6}$	503.3372	86.27	0.26
24	6α-hydroxytriptocalline A	$C_{28}H_{44}O_5$	461.1522	89.95	-0.1
25	Mayteine	$C_{43}H_{49}NO_{18}$	868.3025/890.2850	96.35	0.61
26	9'-O-furanoylwilfordine	$C_{48}H_{51}NO_{21}$	978.3053/1000.2856	99.92	0.53
27	Orthosphenic acid	$C_{30}H_{48}O_5$	489.3596	105.13	-0.09
28	Kaempferol	$C_{15}H_{18}O_5$	279.1602	107.18	0.24
29	Celastrol	Celastrol $C_{29}H_{38}O_4$ 45		109.83	0.63
30	Salazinic acid	$C_{19}H_{14}O_{10}$	403.2347/425.2162	114.88	0.76
31	Nobiletin	$C_{21}H_{22}O_8$	403.2338/425.2157	116.78	0.52
32	Triptobenzene C	$C_{20}H_{26}O_4$	331.2846/353.2676	120.08	0.94
33	Zhebeiresinol	$C_{14}H_{16}O_{6}$	281.248	123.55	0.19
34	Triptonoterpene	$C_{20}H_{28}O_2$	301.2114	128.28	0.28
35	Demethylregelin	$C_{30}H_{46}O_4$	471.3468	130.45	1.14
36	Salaspermic acid	$C_{30}H_{48}O_4$	473.3486	147.02	0.63
37	Triptoditerpenic acid B	$C_{20}H_{24}O_4$	329.243	150.79	0.36
38	Triptophenolide	$C_{20}H_{24}O_3$	313.3271	159.08	0.44

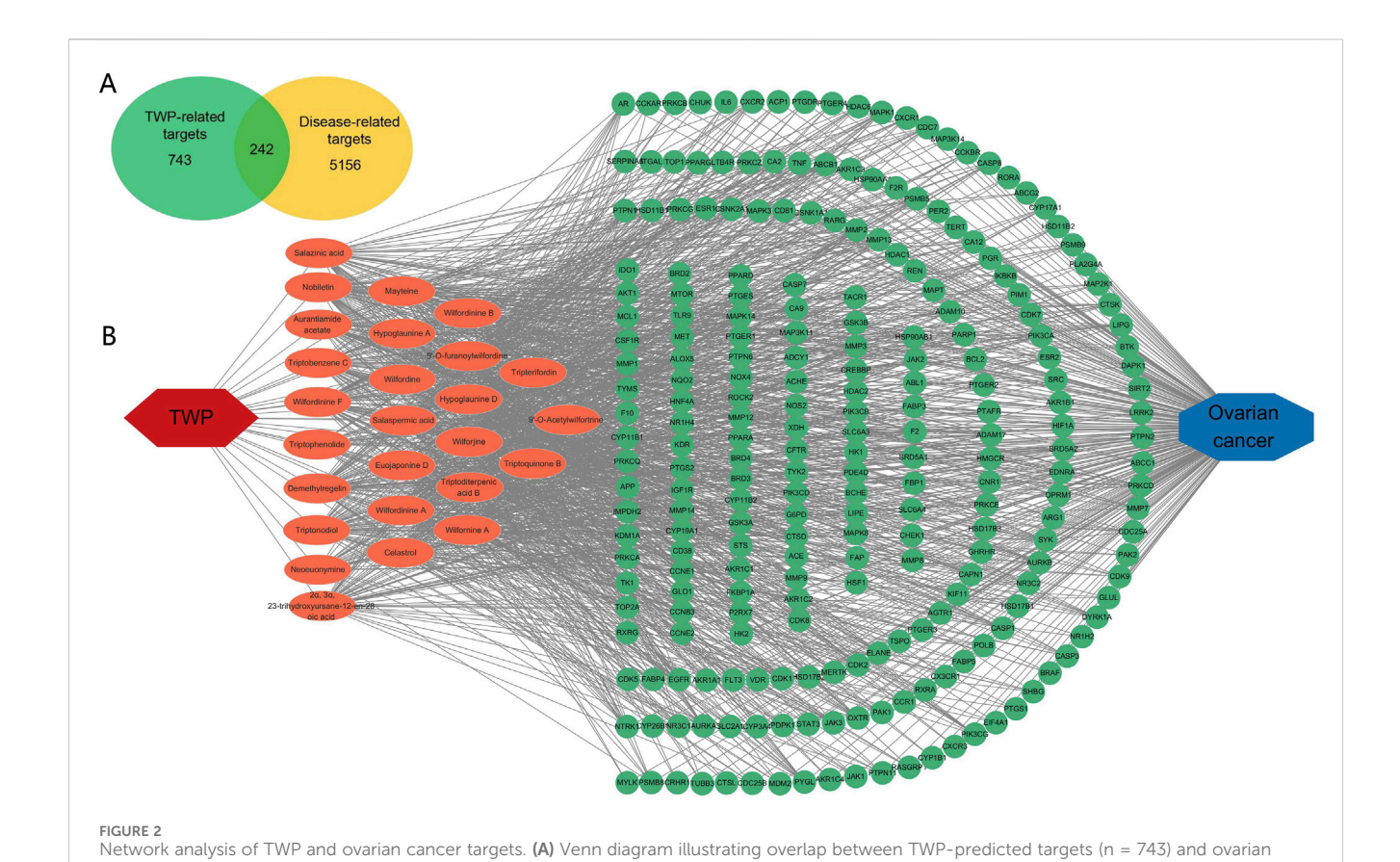


TABLE 2 Top 10 TWP constituents ranked by network degree.

represent targets; edges indicate interactions.

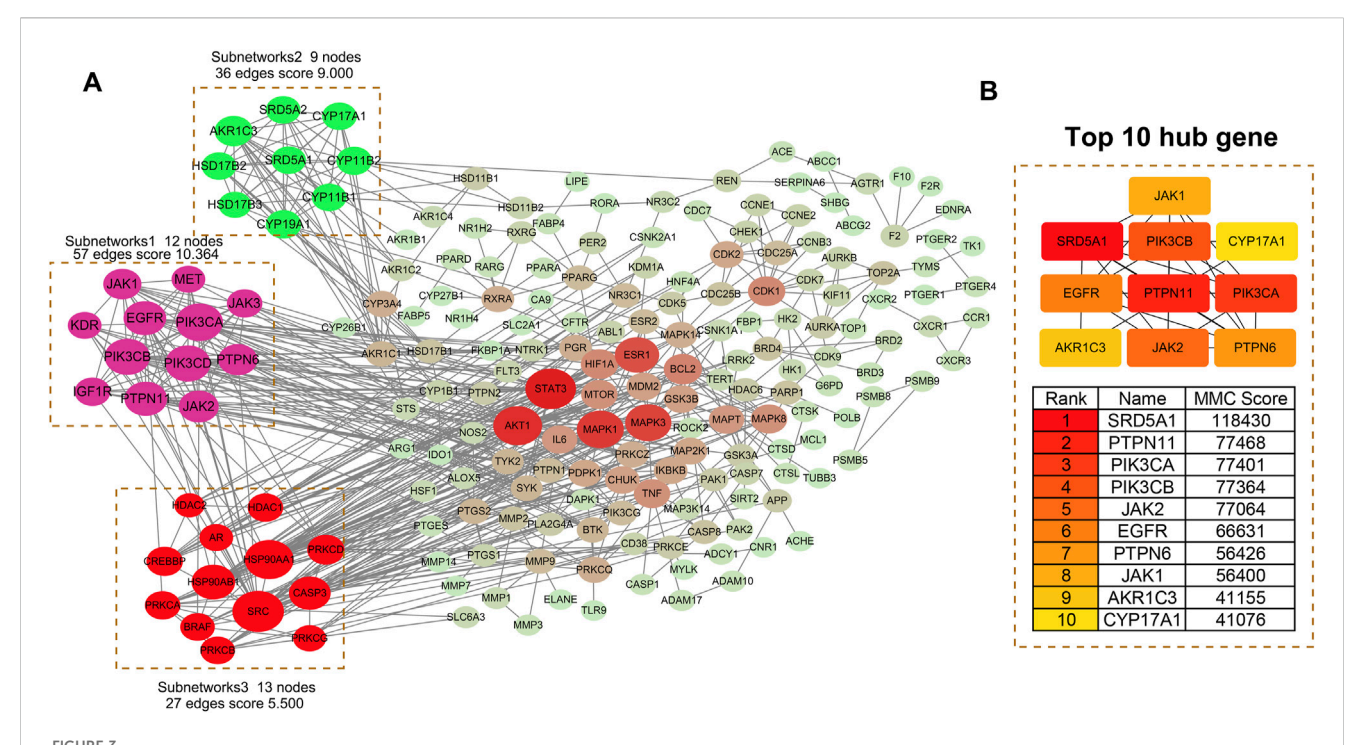
TABLE 2 TOP TO TWY CONSTITUTION ALGICE.						
No.	Compound	Class	Degree	Betweenness centrality		
1	Wilfordinine A	Alkaloids	68	0.0812		
2	Hypoglaunine D	Alkaloids	66	0.0824		
3	Wilfordinine F	Alkaloids	66	0.0520		
4	Mayteine	Alkaloids	66	0.0553		
5	Euojaponine D	Alkaloids	65	0.0676		
6	Wilfornine A	Alkaloids	64	0.0445		
7	Demethylregelin	Triterpenoids	63	0.0838		
8	9'-O-furanoylwilfordine	Alkaloids	59	0.0426		
9	Nobiletin	Flavonoid	58	0.0958		
10	Triptoquinone B	Diterpenoids	56	0.0874		

 $cancer-related genes \ (n=5,156), \ highlighting \ 242 \ shared \ targets. \ \textbf{(B)} \ Compound-target \ network: \ Yellow \ nodes \ represent \ TWP \ compounds; \ blue \ nodes$

The 26 TWP, constituents selected for network pharmacology analysis are categorized into four classes: 13 alkaloids, 6 diterpenoids, 4 triterpenoids, and 3 other compounds. For topological feature comparison, the average degree of alkaloids is 57.3, while that of non-alkaloid compounds (including diterpenoids, triterpenoids, and others) is 31.8. The significantly higher average degree of alkaloids indicates their stronger ability to interact with ovarian cancer-related targets, further supporting their central role in mediating TWP's multi-target therapeutic effects against cisplatin-resistant ovarian cancer.

binding, protein serine/threonine/tyrosine kinase activity (Figure 4B). CC: Cytoplasm, cytosol, plasma membrane, extracellular exosome (Figure 4C). KEGG: Cancer pathways (Pathways in cancer, Prostate cancer), signaling cascades (EGFR

tyrosine kinase inhibitor resistance), and immune regulation (PD-L1/PD-1 checkpoint pathway) (Figure 4D). These results suggest TWP modulates proliferation, apoptosis, inflammation, and immune responses via multi-pathway regulation.



PPI network analysis of TWP targets. (A) Global PPI network with MCODE-identified subnetworks: Subnetwork 1: Signaling pathways (score = 10.364). Subnetwork 2: Steroid hormone biosynthesis (score = 9.000). Subnetwork 3: Inflammation/apoptosis (score = 5.500). Node size reflects connectivity; edges indicate interactions. (B) Top 10 hub genes ranked by degree centrality (interconnected subnetwork).

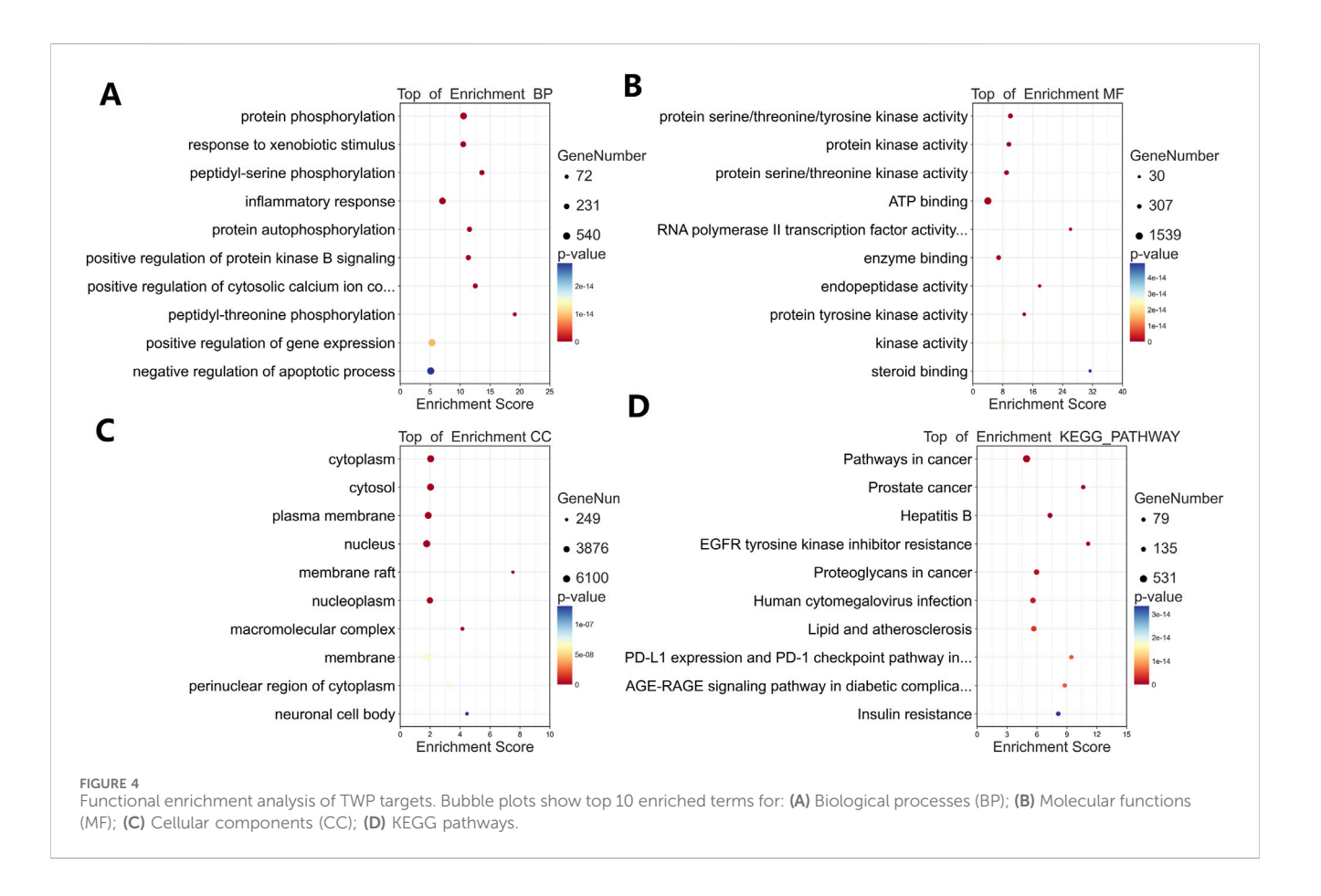
TABLE 3 Top 10 hub genes in the PPI network: functional annotations, targeting compounds, and pathway associations.

Rank	Gene name	MMC score	Targeting compounds	Associated pathways	
1	SRD5A1	41076	12	Steroid hormone biosynthesis, Ovarian steroidogenesis, Metabolic pathways	
2	PTPN11	77468	11	Phospholipase D signaling pathway, Ras signaling pathway, EGFR tyrosine kinase inhibitor resistance	
3	PIK3CA	77401	10	FoxO signaling pathway, Phospholipase D signaling pathway, Pancreatic cancer, Endomet cancer	
4	PIK3CB	77364	11	Phospholipase D signaling pathway, Pancreatic cancer, Chemokine signaling pathway	
5	JAK2	77064	8	JAK-STAT signaling pathway, Prolactin signaling pathway, Necroptosis, Pathways in cancer	
6	EGFR	66631	12	ErbB signaling pathway, Proteoglycans in cancer, EGFR tyrosine kinase inhibitor resistance, Bladder cancer	
7	PTPN6	56426	6	B cell receptor signaling pathway, Natural killer cell mediated cytotoxicity, PD-L1 expression and PD-1 checkpoint pathway in cancer	
8	JAK1	56400	5	JAK-STAT signaling pathway, Necroptosis, Measles, Th17 cell differentiation	
9	AKR1C3	41155	6	Steroid hormone biosynthesis, Ovarian steroidogenesis, Metabolic pathways	
10	CYP17A1	41066	4	Steroid hormone biosynthesis, Ovarian steroidogenesis, Metabolic pathways, Cortisol synthesis and secretion	

3.6 Microarray validation of core targets in clinical datasets

Four independent ovarian cancer microarray datasets (GSE18520, GSE26712, GSE27651, GSE54388) were analyzed to validate the clinical relevance of hub genes. Differentially expressed genes (DEGs) were identified using stringent criteria (adjusted p <

0.05, $|\log 2(FC)| \ge 1$), and volcano plots were generated to visualize the distribution of gene expression changes (Figure 5). The analysis revealed substantial transcriptional alterations across datasets, with 723–3,254 upregulated and 1,296–3,568 downregulated genes per dataset. Among the top 10 hub genes, five core targets (PTPN11, JAK2, EGFR, SRD5A1, and JAK1) demonstrated consistent differential expression in ≥ 2 datasets (Table 4). These five genes,



which demonstrated both network centrality and differential expression in clinical samples, were designated as core targets for subsequent molecular docking analysis. Their differential expression patterns in ovarian cancer tissues suggest potential roles in disease pathogenesis and progression, further supporting their relevance as therapeutic targets for TWP.

3.7 Molecular docking validation of TWP active constituents against core targets

To systematically evaluate the binding potential of representative TWP constituents toward the five core targets predicted by network pharmacology (EGFR, JAK1, JAK2, PTPN11, and SRD5A1), molecular docking was performed with AutoDock Vina for the ten highest-connected TWP compounds. Binding free energy (ΔG) ≤ -5 kcal/mol was set as the threshold for effective binding, and $\Delta G \leq -7$ kcal/mol was defined as strong binding (Ge et al., 2024). Heat-map analysis (Figure 6) revealed that all the compound-target pairs exhibited $\Delta G \leq -5$ kcal/mol, of which 27 pairs reached $\Delta G \leq -7$ kcal/mol, indicating broad and robust binding propensity. Comparative evaluation identified the optimal ligand for each target: EGFR-Wilfordinine A (-9.2 kcal/ mol), JAK1-Mayteine (-8.8 kcal/mol), JAK2-Wilfordinine F (-8.5 kcal/mol), PTPN11-Wilfornine A (-7.8 kcal/mol), SRD5A1-Euojaponine D (-9.5 kcal/mol). Detailed pose analysis (Figure 7) showed that TWP constituents anchor within the catalytic pockets via hydrogen bonding, hydrophobic contacts,

 π - π stacking, and van der Waals forces. Specifically, Wilfordinine A forms key hydrogen bonds with EGFR Lys745 and Met793, whereas Euojaponine D establishes an extensive hydrophobic network within the SRD5A1 binding cavity. These findings corroborate the network-predicted targets and provide structural insights into the multitarget molecular basis underlying TWP efficacy in ovarian cancer therapy.

3.8 MD simulation analysis

To probe the thermodynamic stability and conformational dynamics of the top-ranked complexes, 100-ns all-atom MD simulations were performed for the five optimal pairs identified in Section 3.7: EGFR-Wilfordinine A, JAK1-Mayteine, JAK2-Wilfordinine F, PTPN11-Wilfornine A, and SRD5A1-Euojaponine D. Structural stability and residue flexibility were quantified via RMSD and RMSF, respectively. RMSD trajectories (Figure 8, left) indicate rapid convergence to equilibrium for all systems. EGFR-Wilfordinine A and JAK1-Mayteine plateau at ~0.5-0.6 nm after 15-20 ns, whereas JAK2-Wilfordinine F stabilizes similarly at ~0.6 nm PTPN11-Wilfornine A exhibits the lowest RMSD (~0.35 nm), reflecting a compact binding mode. SRD5A1-Euojaponine D undergoes a 30ns relaxation phase before stabilizing at ~0.45 nm, consistent with initial pocket remodeling. Ligand RMSDs remain <0.2 nm throughout, confirming persistent binding poses. RMSF profiles (Figure 8, right) reveal that flexible loops and termini

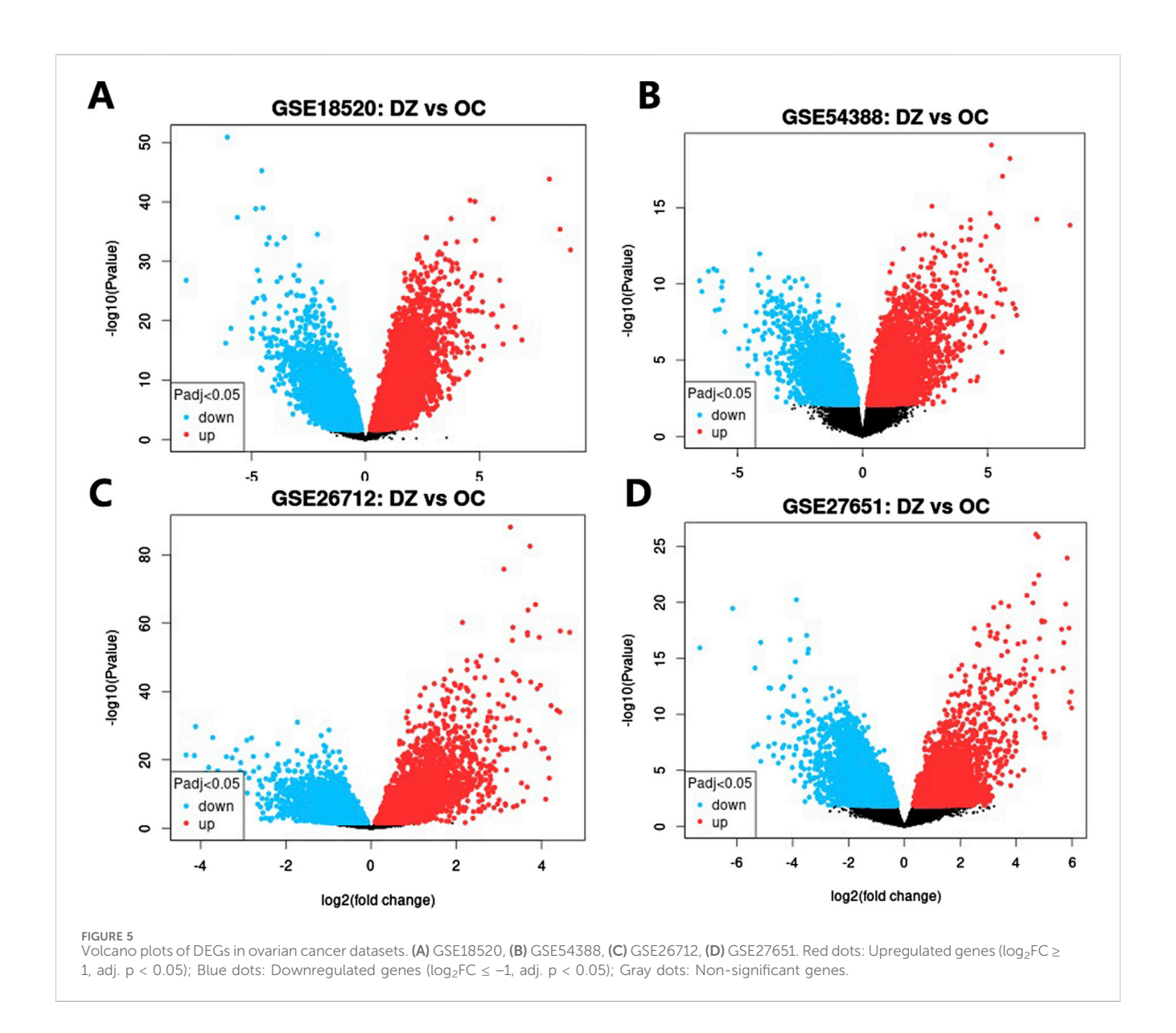


TABLE 4 Integrated analysis of GEO datasets and core target gene expression.

Dataset	Platform	Control	Affected	Downregulated	Stable	Upregulated	DEGs of core target genes
GSE54388	GPL570	6	16	1,877	2,884	1,266	PTPN11
GSE27651	GPL570	6	43	3,568	4,805	3,254	JAK2, EGFR, SRD5A1
GSE18520	GPL570	10	53	2,671	10,110	2,984	PTPN11, JAK2, SRD5A1, JAK1
GSE26712	GPL570	10	185	1,296	6,678	723	EGFR

account for most residue mobility, while catalytic cores retain rigidity. EGFR shows flexibility peaks at residues 50-75, 175-200 and 280-300; JAK1 and JAK2 exhibit elevated N-terminal and loop fluctuations; PTPN11 displays moderate, uniform mobility; SRD5A1 presents pronounced flexibility in residues 50-100 and 350-450. Collectively, the converged RMSD and restrained RMSF of binding-site residues corroborate the docking-derived poses and underscore the reliability of the predicted TWP-target interactions.

3.9 TWP suppresses ovarian cancer cell viability

The predicted antitumor activity of TWP was first verified by CCK-8 assay in SKOV3 and cisplatin-resistant A2780/DDP cells. After 24 h exposure, TWP induced a concentration-dependent reduction in viability in both lines (Figure 9). In SKOV3 cells, 5, 10 and 20 μ g/mL TWP decreased viability to 86.2% \pm 3.1%, 71.5% \pm 2.8% and 52.3% \pm 3.5%, respectively. Comparable efficacy was

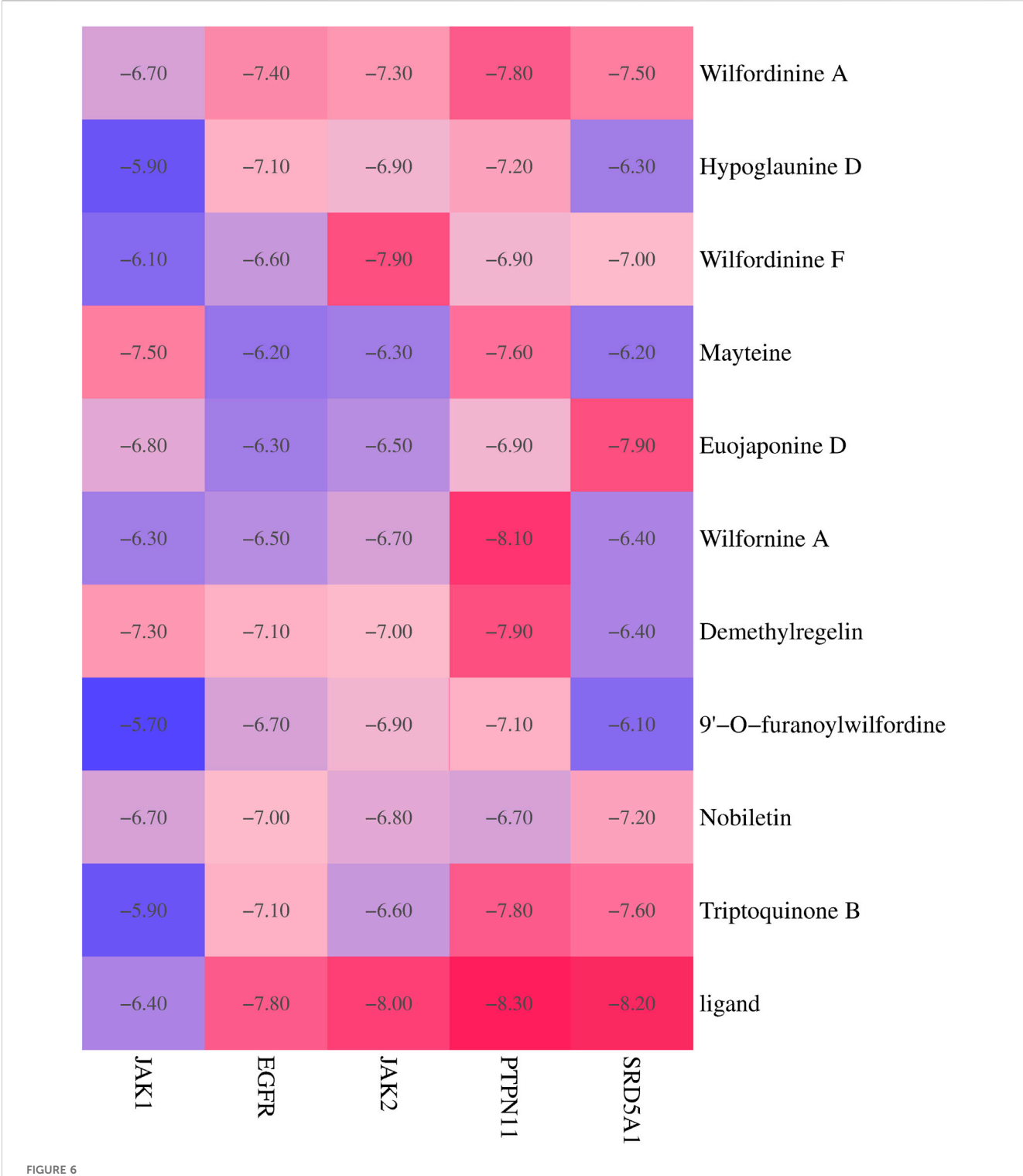


FIGURE 6
Heat map of docking energies (kcal/mol) between the top 10 TWP constituents and five core targets. Darker red indicates stronger binding.

observed in A2780/DDP cells (85.2% \pm 3.1%, 68.5% \pm 2.8% and 50.3% \pm 3.5%). As expected, 10 μM cisplatin strongly inhibited SKOV3 cells (33.3% \pm 2.4% viability) but exerted minimal cytotoxicity on A2780/DDP cells (92.5% \pm 3.7%), confirming drug resistance. Notably, TWP retained potent activity against the resistant line, underscoring its therapeutic potential for cisplatin-refractory ovarian cancer.

3.10 TWP induces apoptosis in cisplatinresistant cells

To determine whether TWP triggers programmed cell death in the cisplatin-resistant A2780/DDP line, Annexin V-FITC/PI flow cytometry and Western blot were performed. After 24 h exposure, TWP dose-dependently increased total apoptosis (early + late) from

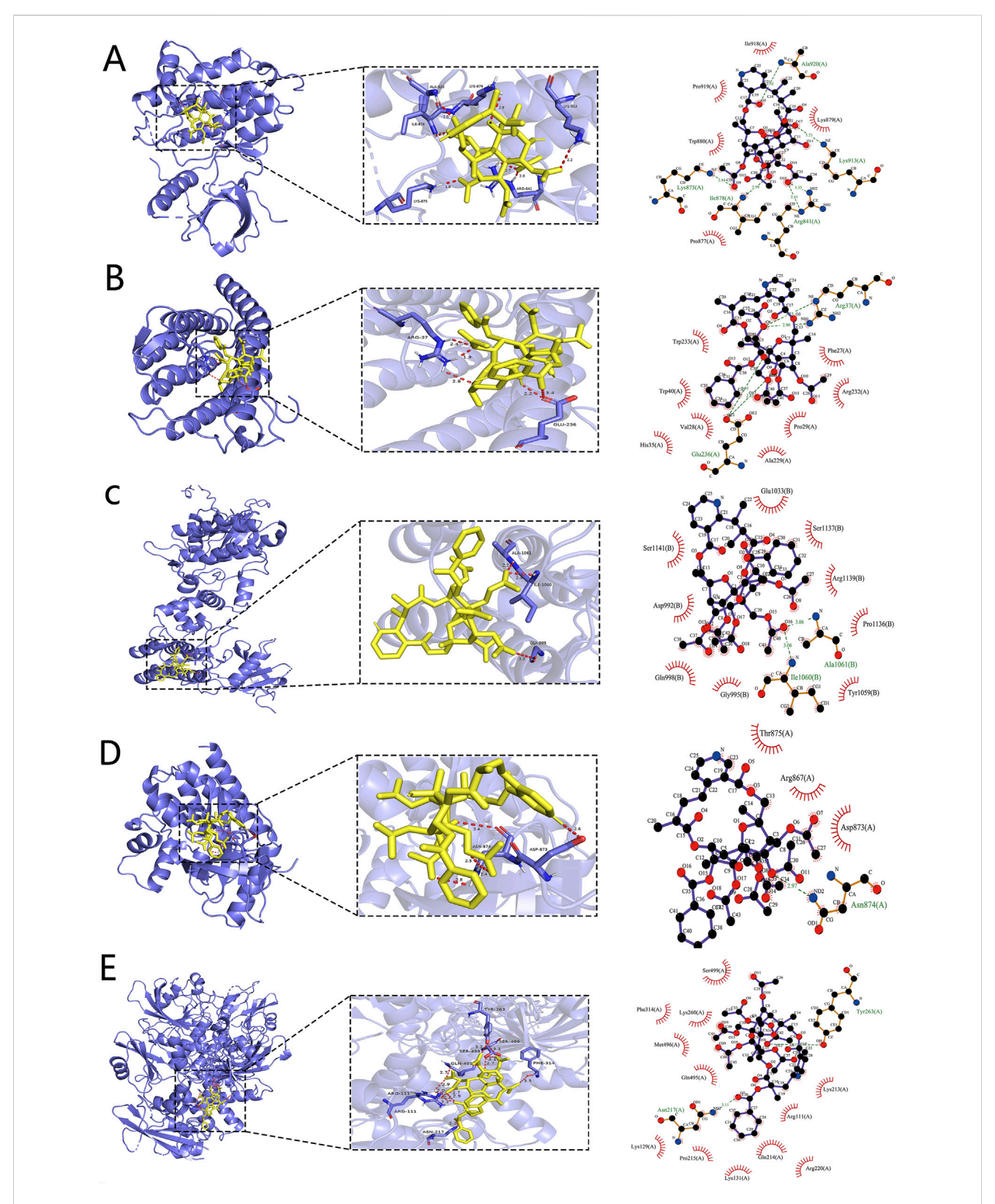
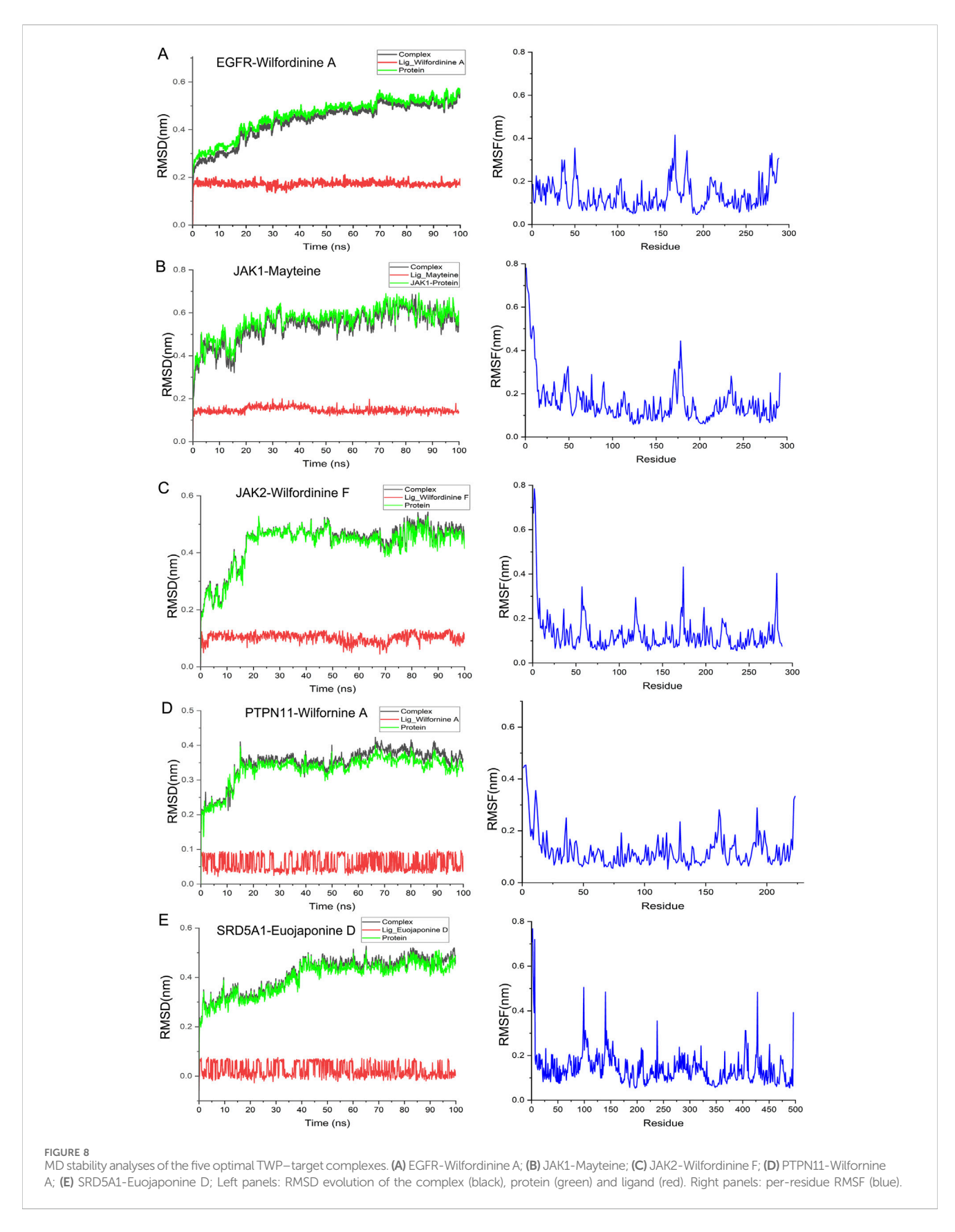
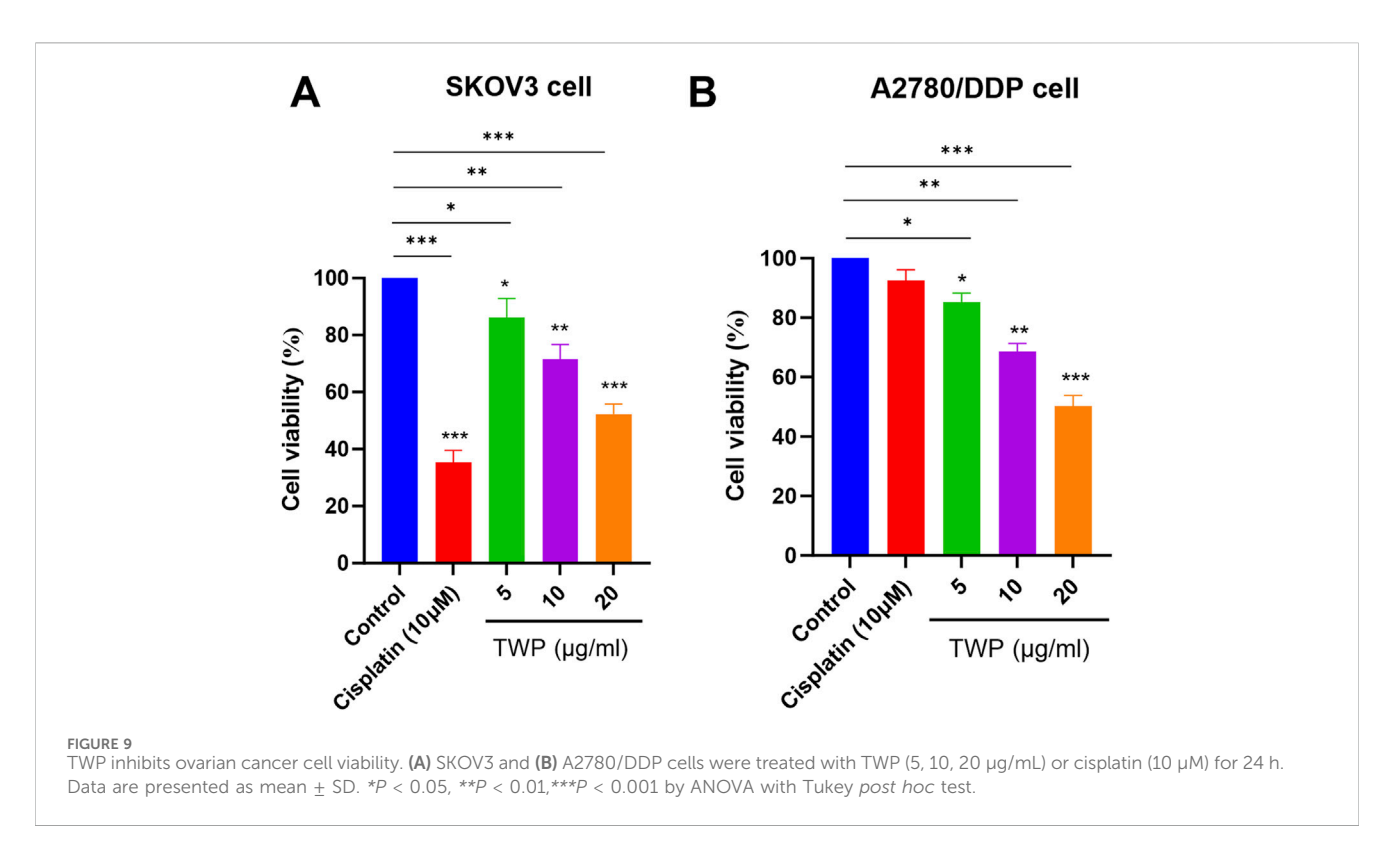


FIGURE 7
Representative binding poses of the optimal TWP ligands in the active sites of core targets. (A) EGFR-Wilfordinine A; (B) JAK1-Mayteine; (C) JAK2-Wilfordinine F; (D) PTPN11-Wilfornine A; (E) SRD5A1-Euojaponine D. Left panels: overall protein cartoon (blue) with ligand (yellow sticks) and binding-site box (dashed line). Middle panels: close-up 3D interactions (hydrogen bonds as dashed yellow lines, distances in Å). Right panels: 2D interaction diagrams.



6.65% (control) to 14.57%, 26.63% and 55.9% at 5, 10 and 20 $\mu g/mL$, respectively (Figure 10A). Western blot analysis revealed a corresponding molecular signature: Bax and cleaved Caspase-3

were upregulated, whereas Bcl-2 was downregulated, yielding a marked reduction in the Bcl-2/Bax ratio (Figure 10B). These data demonstrate that TWP overcomes cisplatin resistance by shifting the



Bcl-2 family balance and activating the Caspase-3 mediated intrinsic apoptotic pathway.

3.11 TWP suppresses EGFR/JAK/ PTPN11 signaling in cisplatin-resistant A2780/DDP cells

To verify the network-pharmacology predictions, A2780/DDP cells were treated with TWP (0–20 µg/mL) for 24 h and analyzed by Western blot analysis. As shown in Figure 11, TWP produced a concentration-dependent reduction in the phosphorylated forms of EGFR, JAK1, JAK2 and PTPN11; significant inhibition was evident at 5 µg/mL and maximal at 20 µg/mL (P < 0.001). Total EGFR and JAK2 levels remained unchanged, whereas total JAK1 and PTPN11 were modestly decreased only at 20 µg/mL (P < 0.05). SRD5A1 expression declined markedly at the same dose (P < 0.05). These results demonstrate that TWP primarily inactivates upstream kinases/phosphatases through de-phosphorylation, with secondary downregulation of select targets at higher concentrations, thereby disrupting multiple pro-growth circuits in cisplatin-resistant ovarian cancer cells.

3.12 TWP inhibits PI3K-AKT, JAK-STAT, and ERK-MAPK signaling

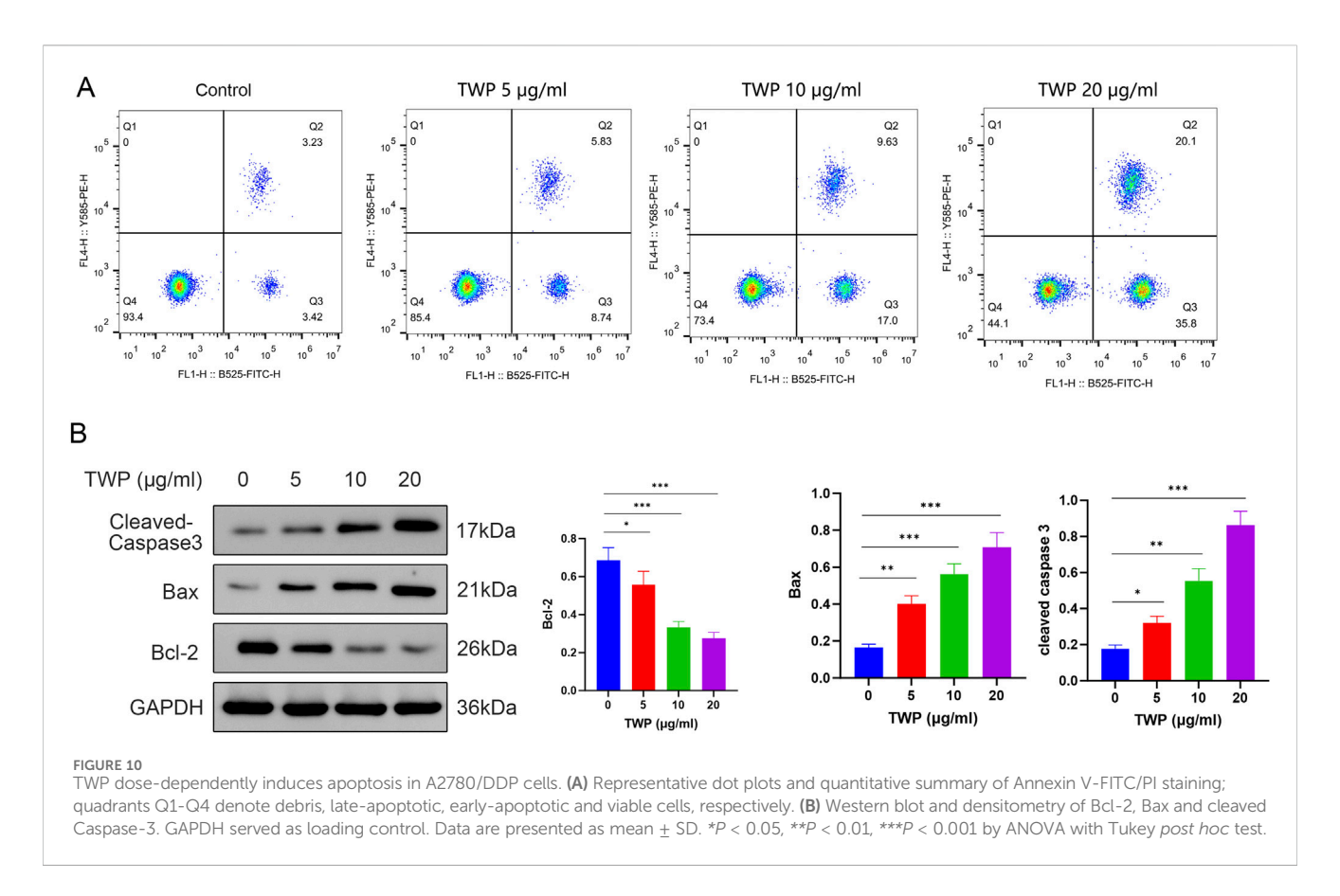
To verify the downstream consequences of TWP-mediated inhibition of upstream signaling molecules described in section 2.11, we investigated the effects of TWP on three major signaling cascades: PI3K-AKT, JAK-STAT, and ERK-MAPK pathways. Western blot analysis (Figure 12) demonstrated that TWP treatment resulted in a concentration-dependent decrease in the phosphorylation levels of Akt,

STAT3, and ERK1/2 in A2780/DDP cells. Importantly, total protein levels of Akt, STAT3 and ERK1/2 remained unaltered across the entire concentration range, confirming that TWP modulates pathway activity through post-translational de-phosphorylation rather than transcriptional or translational repression. These results provide direct experimental evidence that TWP simultaneously suppresses the activation of these three critical pro-survival signaling pathways in cisplatin-resistant ovarian cancer cells.

4 Discussion

Ovarian cancer resistance to platinum-based chemotherapy represents a multifactorial process involving dysregulated DNA repair, altered drug transport, and aberrant survival signaling (Xiong et al., 2024). Conventional single-target agents often fail due to tumor heterogeneity and compensatory pathway activation, highlighting the need for multitarget strategies (Doostmohammadi et al., 2024). Our integrated approach, bridging UPLC/Q-TOF-MS analysis with computational prediction and experimental validation, has elucidated a coherent mechanistic framework for TWP's ability to overcome this resistance.

We identified that alkaloids represent a major bioactive class within TWP and demonstrated that they execute a multi-pronged attack on a hub of signaling proteins crucial for chemoresistance. This finding expands the current understanding of Tripterygium's therapeutic potential, suggesting that alkaloids—alongside diterpenoids—may contribute significantly to its anti-tumor activity through complementary mechanisms. Emerging evidence indicates that alkaloids exhibit distinct pharmacokinetic advantages, including enhanced bioavailability and multi-target modulation of apoptosis, oxidative stress, and chemosensitization pathways (Mondal et al., 2019; Olofinsan et al., 2023).



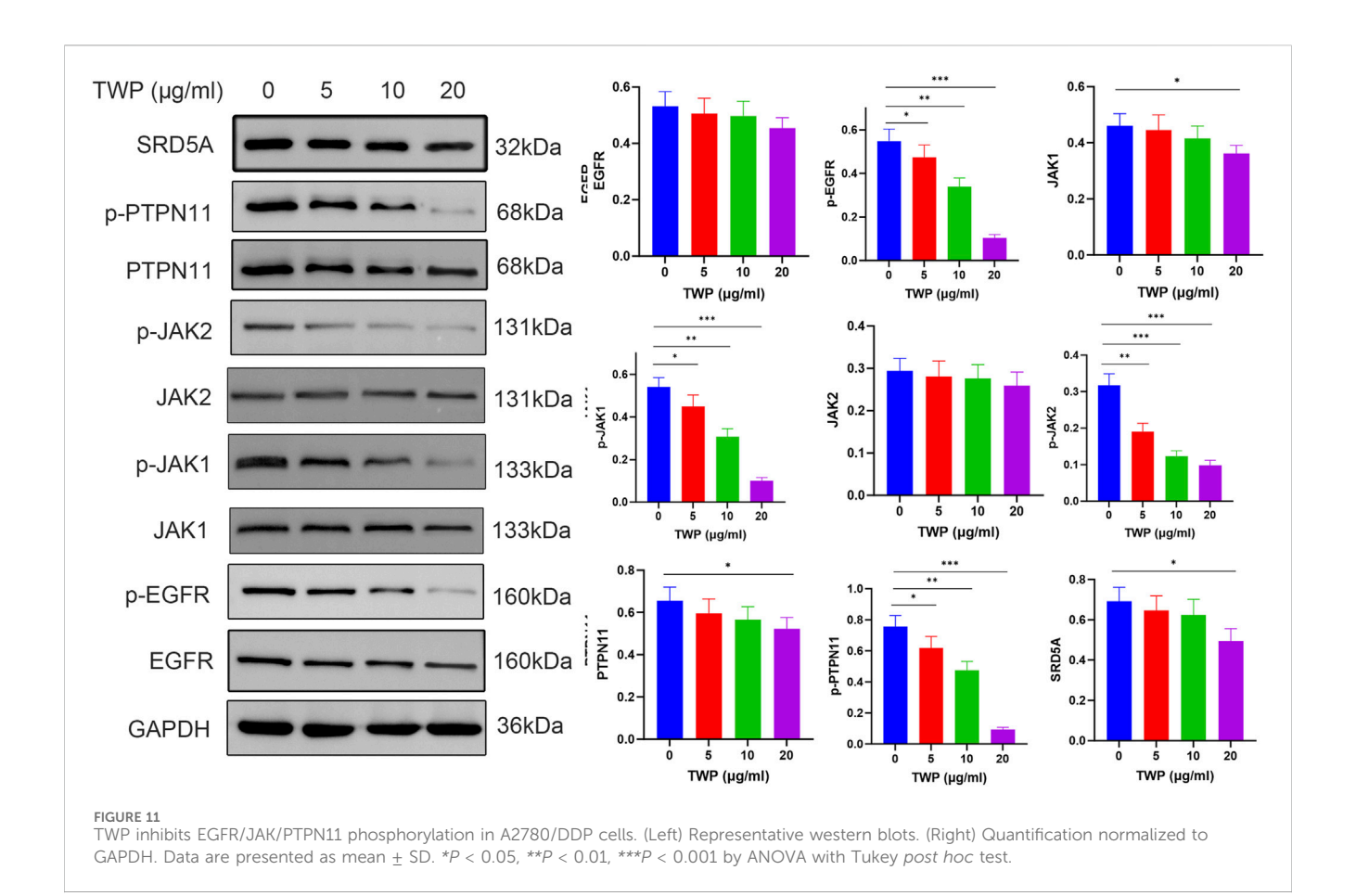
Our investigation revealed that TWP's efficacy is driven by its ability to modulate five core targets-EGFR, JAK1, JAK2, PTPN11, and SRD5A1—which our analysis showed to be dysregulated in clinical ovarian cancer datasets. The EGFR-PI3K-AKT and JAK-STAT pathways are frequently co-activated in platinum-resistant ovarian cancer, creating redundant survival signals that limit single-agent efficacy (Zhao et al., 2021). Simultaneously targeting these parallel pathways has emerged as a rational strategy to overcome therapeutic escape (Wen et al., 2015). The identification of PTPN11 and SRD5A1 as additional key targets represents a significant advance. PTPN11 (SHP2), a critical node in receptor tyrosine kinase (RTK) signaling, is consistently upregulated in ovarian cancer and promotes tumor progression via the PI3K-AKT and ERK-MAPK pathways (Fedele et al., 2018; Cao et al., 2022). Our data showing TWP-mediated PTPN11 inhibition suggests a mechanism to disrupt these oncogenic cascades, potentially circumventing resistance. Similarly, TWP's suppression SRD5A1 may attenuate androgen signaling, which contributes to progression in a significant subset of ovarian cancers, offering a novel strategy to counteract hormone-mediated chemoresistance (Mizushima and Miyamoto, 2019; Chung et al., 2021).

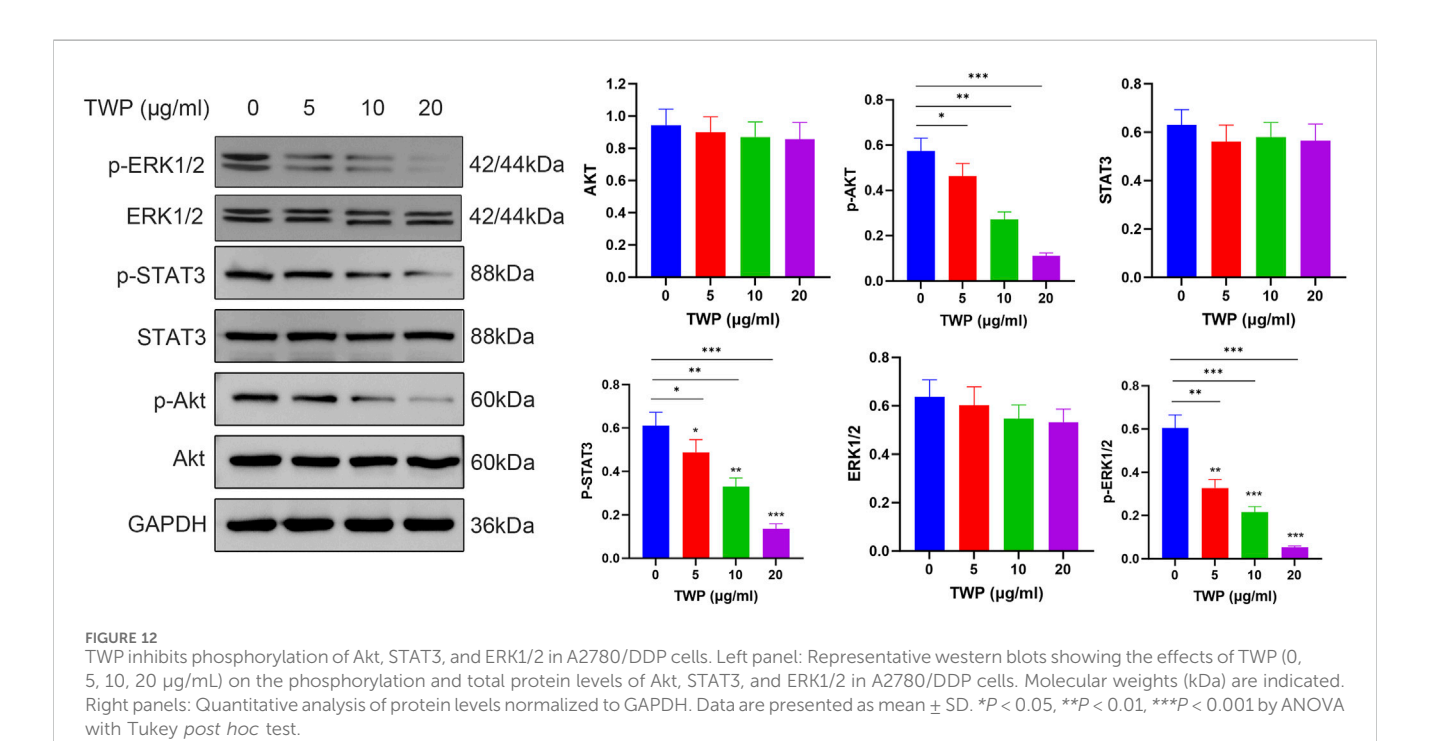
The consequence of this upstream, multi-target engagement is a profound and coordinated collapse of downstream signaling pathways. The observed blockade of Akt, STAT3, and ERK phosphorylation is not merely a downstream effect but the functional nexus of TWP's anticancer action. By curtailing Akt activation, TWP deprives tumor cells of a critical pro-survival hub, re-sensitizing them to cisplatin-induced apoptosis (Li et al., 2024). Similarly, TWP-mediated inhibition of STAT3 phosphorylation dismantles a key driver of immune evasion, metastasis, and cancer stemness (Liu et al., 2025). Finally, the

suppression of ERK phosphorylation interrupts the canonical MAPK cascade, blunting mitogenic signals (Lucas et al., 2022). This multi-node suppression generates a synergistic attenuation of the transcriptional programs governing proliferation and survival, which is the cornerstone of overcoming chemoresistance.

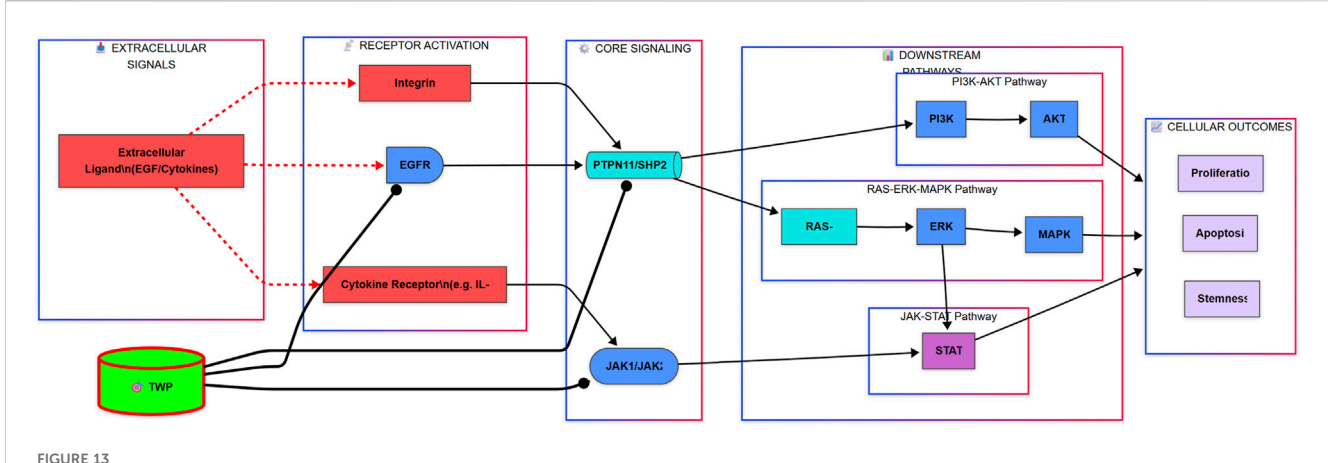
As illustrated in the comprehensive signaling diagram (Figure 13), our findings paint a cohesive picture. TWP alkaloids act as inhibitors at the receptor and signal integration level, targeting EGFR, JAK1/2, and the pivotal phosphatase PTPN11/SHP2. This action blocks signals emanating from growth factors (e.g., EGF) and cytokines (e.g., IL-6), leading to the simultaneous shutdown of three distinct but interconnected oncogenic cascades: the JAK-STAT pathway, the Ras-ERK-MAPK pathway, and the PI3K-AKT pathway. The ultimate result is the inhibition of key malignant phenotypes, including proliferation and stemness, and the induction of apoptosis, thereby restoring cisplatin sensitivity.

The clinical implications of these findings are substantial, especially given the suboptimal outcomes in platinum-resistant ovarian cancer (PROC) (Eskander et al., 2023; Leung and Konstantinopoulos, 2021; Naumann and Coleman, 2011) The ability of TWP to simultaneously inhibit EGFR, JAK-STAT, PTPN11, and androgen signaling pathways suggests strong potential for synergy with existing targeted therapies. For instance, TWP-mediated PTPN11/SHP2 inhibition may prevent resistance to EGFR inhibitors (e.g., osimertinib) by blocking RAS-ERK-MAPK reactivation (Chen et al., 2024; Scheiter et al., 2024). Its suppression of PI3K-AKT signaling may synergize with PARP inhibitors by downregulating BRCA expression and exacerbating DNA repair deficiency, a strategy shown to be effective in platinum-resistant models (Bhamidipati et al., 2023; Xu et al., 2022).





The alkaloids we identified belong to a class of natural products that have been a cornerstone of cancer chemotherapy for decades, including vinca alkaloids and camptothecin derivatives (Olofinsan et al., 2023; Mondal et al., 2019). The strong binding affinities and stable interactions observed in our molecular dynamics simulations provide a structural blueprint for potentially optimizing these



Proposed Mechanism for TWP-Mediated Reversal of Cisplatin Resistance in Ovarian Cancer. The alkaloid components of TWP act as multi-target inhibitors, engaging upstream regulators including EGFR, Cytokine Receptors (via JAK1/JAK2), and the critical signal integrator PTPN11/SHP2. This coordinated inhibition blocks signal transduction through three major oncogenic pathways: the JAK-STAT, RAS-ERK-MAPK, and PI3K-AKT cascades. Consequently, this leads to the suppression of pro-survival outputs such as proliferation and stemness, while promoting apoptosis, ultimately restoring cellular sensitivity to cisplatin.

natural compounds into multi-target inhibitors with improved pharmacokinetic profiles, following the successful trajectory of many other plant-derived anti-cancer agents.

Crucially, TWP is already an approved prescription drug in China for inflammatory and autoimmune indications. This existing clinical foundation confers notable translational advantages over *de novo* chemical entities: established manufacturing and quality control, known safety management, and clinical accessibility. Mechanistic elucidation of its anti-tumor actions provides a rational basis for indication expansion via drug repurposing, potentially accelerating its path into oncology, where platinum-resistant ovarian cancer represents a clear unmet need. Such a "mechanism-to-medicine" trajectory—grounded in multi-target network disruption—supports pragmatic clinical exploration, including rational combinations with targeted or DNA damage response agents.

5 Limitations

Despite these advances, several limitations warrant acknowledgment. First, our validation was restricted to in vitro models; future studies must employ patient-derived xenografts (PDX) or organoids to recapitulate the complex tumor microenvironment (Yoshida, 2020). Second, our in vitro validation was conducted using the total TWP extract rather than an alkaloidenriched fraction or isolated compounds. This approach was chosen for its direct clinical relevance, as TWP is the approved pharmaceutical preparation. However, this experimental design means that while our integrated in silico and experimental evidence strongly points to alkaloids as key mediators, we cannot definitively attribute the observed anti-tumor effects solely to this chemical class. Consequently, the precise relative contributions of individual compounds and their potential synergies—both among alkaloids and between alkaloids and other constituents like diterpenoids-remain unresolved (Wu et al., 2022). Future work with isolated active alkaloids is necessary to deconstruct these complex interactions. Third, the heterogeneity of ovarian cancer subtypes was not addressed, and validation in non-serous carcinomas is an essential next step.

6 Conclusion

This study proposes a mechanism potentially centered on alkaloid constituents by which TWP may help overcomes cisplatin resistance in ovarian cancer. Integrated computational analyses and in vitro assays suggest that TWP engages and EGFR, JAK1, JAK2, inactivates and PTPN11, while downregulating SRD5A1, thereby coordinating suppression of PI3K-AKT, JAK-STAT, and ERK-MAPK signaling. The resulting disruption of redundant survival circuits is associated with apoptosis induction and re-sensitization of resistant cells. While non-alkaloid constituents may also contribute to these effects, the findings provide strong, albeit indirect, support for an alkaloid-driven multi-target synergy. These mechanistic insights not only rationalize the observed anti-tumor activity but also support the potential clinical repurposing of an approved medicine toward oncology indications, and highlight the need for future validation using alkaloid-enriched preparations or isolated monomers.

Data availability statement

The original contributions presented in the study are included in the article/Supplementary Material, further inquiries can be directed to the corresponding author; GEO datasets used are GSE18520, GSE54388, GSE26712, GSE27651.

Author contributions

BL: Conceptualization, Funding acquisition, Supervision, Validation, Writing – original draft, Writing – review and editing. MZ: Investigation, Methodology, Software,

Writing – original draft. YW: Conceptualization, Data curation, Formal Analysis, Investigation, Methodology, Writing – original draft, Writing – review and editing.

Funding

The author(s) declare that financial support was received for the research and/or publication of this article. This research was funded by the Fujian Provincial Joint Fund for Science and Technology Innovation (No.2020Y9041).

Conflict of interest

The authors declare that the research was conducted in the absence of any commercial or financial relationships that could be construed as a potential conflict of interest.

References

Bhamidipati, D., Haro-Silerio, J. I., Yap, T. A., and Ngoi, N. (2023). PARP inhibitors: enhancing efficacy through rational combinations. *Br. J. Cancer.* 129 (6), 904–916. doi:10.1038/s41416-023-02326-7

Cao, Y., Duan, H., Su, A., Xu, L., and Lai, B. (2022). A pan-cancer analysis confirms PTPN11's potential as a prognostic and immunological biomarker. *Aging (Albany NY)* 14 (13), 5590–5610. doi:10.18632/aging.204171

Chen, X., Keller, S. J., Hafner, P., Alrawashdeh, A. Y., Avery, T. Y., Norona, J., et al. (2024). Tyrosine phosphatase PTPN11/SHP2 in solid tumors - bull's eye for targeted therapy? *Front. Immunol.* 15, 1340726. doi:10.3389/fimmu.2024.1340726

Chung, W., Chen, L., Chang, W., Su, S., Hung, Y., and Ma, W. (2021). Androgen/androgen receptor signaling in ovarian cancer: molecular regulation and therapeutic potentials. *Int. J. Mol. Sci.* 22 (14), 7748. doi:10.3390/ijms22147748

Doostmohammadi, A., Jooya, H., Ghorbanian, K., Gohari, S., and Dadashpour, M. (2024). Potentials and future perspectives of multi-target drugs in cancer treatment: the next generation anti-cancer agents. *Cell Commun. Signal.* 22 (1), 228. doi:10.1186/s12964-024-01607-9

Eskander, R. N., Moore, K. N., Monk, B. J., Herzog, T. J., Annunziata, C. M., O'Malley, D. M., et al. (2023). Overcoming the challenges of drug development in platinum-resistant ovarian cancer. *Front. Oncol.* 13, 1258228. doi:10.3389/fonc.2023.1258228

Fedele, C., Ran, H., Diskin, B., Wei, W., Jen, J., Geer, M. J., et al. (2018). SHP2 inhibition prevents adaptive resistance to MEK inhibitors in multiple cancer models. *Cancer Discov.* 8 (10), 1237–1249. doi:10.1158/2159-8290.CD-18-0444

Ge, J., Ye, L., Cheng, M., Xu, W., Chen, Z., and Guan, F. (2024). Preparation of microgels loaded with lycopene/NMN and their protective mechanism against acute liver injury. *Food Funct.* 15 (2), 809–822. doi:10.1039/d3fo03293k

Leung, S. O. A., and Konstantinopoulos, P. A. (2021). Advances in the treatment of platinum resistant epithelial ovarian cancer: an update on standard and experimental therapies. *Expert Opin. Investig. Drugs* 30 (7), 695–707. doi:10.1080/13543784.2021.1939305

Li, J., Chen, M., Huang, D., Li, Z., Chen, Y., Huang, J., et al. (2024). Inhibition of selenoprotein I promotes ferroptosis and reverses resistance to platinum chemotherapy by impairing akt phosphorylation in ovarian cancer. *MedComm* 5 (12), e70033. doi:10. 1002/mco2.70033

Liu, X., Qi, M., Li, X., Wang, J., and Wang, M. (2023). Curcumin: a natural organic component that plays a multi-faceted role in ovarian cancer. *J. Ovarian Res.* 16 (1), 47. doi:10.1186/s13048-023-01120-6

Liu, C., Yin, Q., Wu, Z., Li, W., Huang, J., Chen, B., et al. (2025). Inflammation and immune escape in ovarian cancer: pathways and therapeutic opportunities. *J. Inflamm. Res.* 18, 895–909. doi:10.2147/JIR.S503479

Lucas, R. M., Luo, L., and Stow, J. L. (2022). ERK1/2 in immune signalling. *Biochem. Soc. Trans.* 50 (5), 1341–1352. doi:10.1042/BST20220271

Ma, B., Zhong, Y., Chen, R., Zhan, X., Huang, G., Xiong, Y., et al. (2023). Tripterygium glycosides reverse chemotherapy resistance in ovarian cancer by targeting the NRF2/GPX4 signal axis to induce ferroptosis of drug-resistant human epithelial ovarian cancer cells. *Biochem. Biophys. Res. Commun.* 665, 178–186. doi:10.1016/j.bbrc.2023.04.111

Mizushima, T., and Miyamoto, H. (2019). The role of androgen receptor signaling in ovarian cancer. $\it Cells~8~(2),~176.~doi:10.3390/cells8020176$

Generative Al statement

The author(s) declare that no Generative AI was used in the creation of this manuscript.

Any alternative text (alt text) provided alongside figures in this article has been generated by Frontiers with the support of artificial intelligence and reasonable efforts have been made to ensure accuracy, including review by the authors wherever possible. If you identify any issues, please contact us.

Publisher's note

All claims expressed in this article are solely those of the authors and do not necessarily represent those of their affiliated organizations, or those of the publisher, the editors and the reviewers. Any product that may be evaluated in this article, or claim that may be made by its manufacturer, is not guaranteed or endorsed by the publisher.

Mondal, A., Gandhi, A., Fimognari, C., Atanasov, A. G., and Bishayee, A. (2019). Alkaloids for cancer prevention and therapy: current progress and future perspectives. *Eur. J. Pharmacol.* 858, 172472. doi:10.1016/j.ejphar.2019.172472

Murphy, B., Nasir-Moin, M., von Oiste, G., Chen, V., Riina, H. A., Kondziolka, D., et al. (2021). Patient level simulation and reinforcement learning to discover novel strategies for treating ovarian cancer. arXiv e-prints.

Naumann, R. W., and Coleman, R. L. (2011). Management strategies for recurrent platinum-resistant ovarian cancer. *Drugs* 71 (11), 1397–1412. doi:10.2165/11591720-0000000-000000

Olofinsan, K., Abrahamse, H., and George, B. P. (2023). Therapeutic role of alkaloids and alkaloid derivatives in cancer management. *Molecules* 28 (14), 5578. doi:10.3390/molecules28145578

Scheiter, A., Lu, L., Gao, L. H., and Feng, G. (2024). Complex roles of PTPN11/SHP2 in carcinogenesis and prospect of targeting SHP2 in cancer therapy. *Annu. Rev. Cancer Biol.* 8 (1), 15–33. doi:10.1146/annurev-cancerbio-062722-013740

Wen, W., Wu, J., Liu, L., Tian, Y., Buettner, R., Hsieh, M., et al. (2015). Synergistic anti-tumor effect of combined inhibition of EGFR and JAK/STAT3 pathways in human ovarian cancer. *Mol. Cancer.* 14, 100. doi:10.1186/s12943-015-0366-5

Wu, W., Cheng, R., Boucetta, H., Xu, L., Pan, J., Song, M., et al. (2022). Differences in multicomponent pharmacokinetics, tissue distribution, and excretion of tripterygium glycosides tablets in normal and adriamycin-induced nephrotic syndrome rat models and correlations with efficacy and hepatotoxicity. *Front. Pharmacol.* 13, 910923. doi:10. 3389/fphar.2022.910923

Xiong, Z., Ha, C., Li, R., Wu, M., and Wei, M. (2024). Related clinical factors of platinum-based chemotherapy resistance in patients with epithelial ovarian cancer. *Gynecol. Obstet. Invest.* 89 (6), 469–477. doi:10.1159/000539295

Xu, J., Gao, Y., Luan, X., Li, K., Wang, J., Dai, Y., et al. (2022). An effective AKT inhibitor-PARP inhibitor combination therapy for recurrent ovarian cancer. *Cancer. Chemother. Pharmacol.* 89 (5), 683–695. doi:10.1007/s00280-022-04403-9

Xue, K., Bai, Y., Han, Y., Yao, C., Zhao, Z., Liang, D., et al. (2025). Ginsenoside Rg6 improves cisplatin resistance in epithelial ovarian cancer cells via suppressing fucosylation and inducing autophagy. *Am. J. Chine. Med.* 53 (02), 621–646. doi:10.1142/S0192415X25500247

Yoshida, G. J. (2020). Applications of patient-derived tumor xenograft models and tumor organoids. J. Hematol. Oncol. 13 (1), 4. doi:10.1186/s13045-019-0829-z

Zhan, X., Zuo, Q., Huang, G., Qi, Z., Wang, Y., Zhu, S., et al. (2023). Tripterygium glycosides sensitizes cisplatin chemotherapeutic potency by modulating gut microbiota in epithelial ovarian cancer. *Front. Cell. Infect. Microbiol.* 13, 1236272. doi:10.3389/fcimb.2023.1236272

Zhang, X., Xiong, B., Cheng, Y., Huang, J., Xue, J., Li, X., et al. (2025). Berberine inhibits metastasis of ovarian cancer by blocking lipid metabolism, alleviating aging of adipose tissue and increasing tumor infiltrating immune cells. *Transl. Oncol.* 56, 102380. doi:10.1016/j.tranon.2025.102380

Zhao, J., Tan, W., Zhang, L., Liu, J., Shangguan, M., Chen, J., et al. (2021). FGFR3 phosphorylates EGFR to promote cisplatin-resistance in ovarian cancer. *Biochem. Pharmacol.* 190, 114536. doi:10.1016/j.bcp.2021.114536